Studies for a stand-alone photon trigger based on the total deposited energy and the transverse width of the shower measured in ECAL

Catherine Adloff, Denis Fougeron, Richard Hermel
and Sylvie Rosier-Lees
LAPP, Annecy-Le-Vieux

November 28, 2003

The first proposal of a stand-alone photon trigger for the AMS detector was developed in [1], motivated by the missing data at photon energies between 10 GeV and 300 GeV. The trigger, based exclusively on the answer of the electromagnetic calorimeter ECAL, provides an efficiency of 100 % for photons above 10 GeV with a total rate of 14 Hz.

In this note an upgrade of the trigger algorithm is presented which allows to reach already 97 % efficiency for 3 GeV photons with a total rate below 40 Hz. For completeness the crucial part of the hardware implementation is described in details.

1 Introduction

The ECAL is made of nine 2 cm-thick layers of lead with embedded scintillating fibers, corresponding to a total thickness of 16 radiation lengths. The lateral dimensions are 64.8 cm $\times$ 64.8 cm. Fibers are oriented alternatively in X and Y (Z is the vertical direction) and the signal is read by 2$\times$2 pixel (anodes) photomultipliers (PMT) giving an ultimate granularity of 72 $\times$ 72 cells in the horizontal plane and 18 in the vertical direction. The dynode signals are also included in the readout and provide a granularity of 36 $\times$ 36 $\times$ 9 layers, 4 layers in X direction and 5 in Y.

Using the information of the ECAL it is possible to select non converted photons at the trigger level. This selection must however be fast to fulfill the requirements of the AMS trigger system. A first decision which corresponds to the fast trigger level should be taken in less than 200 ns after the crossing of a photon. With a fixed TDC sampling of the main clock the time decision of the fast trigger is limited in order to keep a high time resolution for the ToF signals (last significant bit around 50 ps). The rate of the gamma trigger at the level 0 should not exceed 1 kHz. After the ECAL fast trigger a window of 900 ns is left for final decision which results in the level 1 trigger decision (1100 ns after the photon crossing). At the level 1 an event is triggered by the stand-alone photon trigger if no ToF trigger occurred. This means that the main background contribution to the rate comes from hadrons outside the ToF acceptance which interact in the ECAL. As the protons flux at the altitude of the ISS is high, especially when AMS is approaching the pole, it is very important to have a large proton rejection factor to keep the ECAL trigger rate low. The contribution to the rate from other types of hadrons like Helium etc should not represent more than 30 % of the proton rate [2]. Finally, the smooth operating of the trigger depends also on its robustness and its easy control in case of problems (noisy channels etc...).

The time constraints for the stand-alone gamma trigger impose to work with fast signals. Only the last dynode of the PMTs were foreseen to have such an additional readout for two reasons: firstly because of the dynode granularity a simple trigger can be built, secondly it represents less danger to degrade the anode signals. The analysis of the ECAL test beam data taken in July 2002 has resulted, amongst others, in an absolute energy calibration of the dynode signals of 1 GeV for 22 mV. This information is crucial for the studies of the trigger technical implementation presented here.

The algorithm presented in [1] was based on the total energy deposited in ECAL and on the transverse width of the shower. The total energy deposited in ECAL is estimated with the analog sum of the dynode signals noted E_{tot}. The transverse width of the shower is represented by the sum of the variables N_X and

N_Y, the number of hit columns in the X and Y direction as illustrated in figure 1. The threshold on E_{tot} was 8 GeV which corresponds to the criteria at the fast trigger level. Final decision at the level 1 was the result of a set of $N_X + N_Y$ cuts in four ranges of E_{tot} (see table 1).

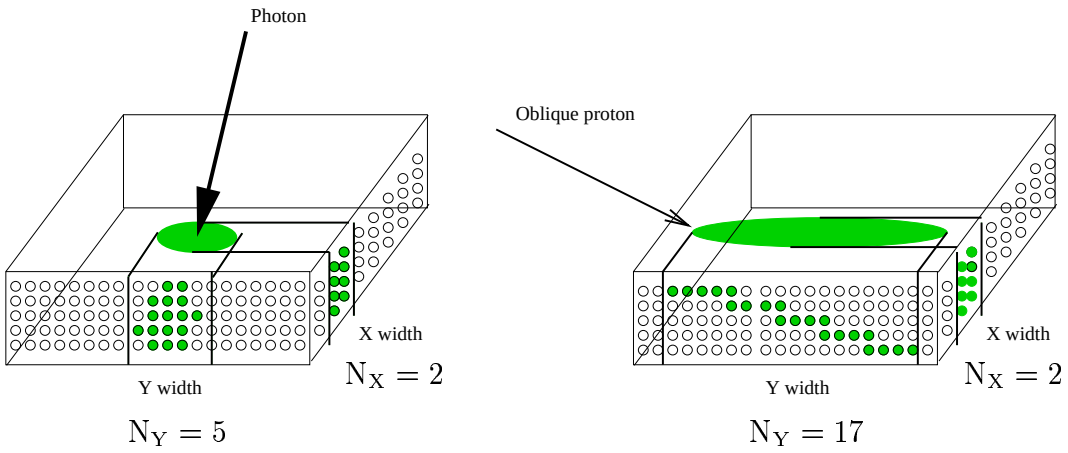

Figure 1: Example of showers for a zenith photon and an oblique proton with corresponding N_X and N_Y.

In [1], N_X and N_Y were calculated by asking at least one dynode in a column to be above a threshold of 100 MeV. The hardware realisation is slightly different (see section 3): first the analog sum of the dynodes in a column is performed and only then the threshold is applied. This configuration is in fact more efficient for incident photons from the zenith and more restrictive on lateral protons. In the present study $N_X + N_Y$ is calculated in agreement with the hardware implementation.

The predominance of GRB at gamma energies lower than 8 GeV and the possibility to measure a lager part of gamma-ray source spectra justifies a trigger with high efficiency for gamma energies as low as possible. In our case it is easy to increase the efficiency for low energy gammas by simply decreasing the total energy threshold and this without affecting the efficiency at high energies. The compromise with the increase of the rate made us choose an energy threshold of 2 GeV together with a readjustment of the trigger algorithm.

The stand-alone photon trigger will react in the same way for electrons and positrons as for photons. Therefore it is possible to recover converted photons in the tracker which are lost by the standard ToF trigger as well as events with back splash electrons which are rejected due to signals in the veto counters [3].

The first section of this note presents the studies performed with the help of the AMS simulation. The methods to evaluate the trigger rate and the photon efficiency are described. Then we introduce an improved algorithm compulsory to lower the total energy threshold down to 2 GeV and we present the results for two different scenarios. Finally the robustness of the trigger algorithm is studied. In the second part the technical issue is developed in details.

2 Simulations

To estimate the performance of the stand-alone gamma trigger three ingredients are necessary: the cosmic proton rate, the proton rejection factor of the trigger algorithm and its efficiency for photons arriving from the zenith.

We have performed the analysis with the proton and photon samples generated at the INFN-Sezione di Pisa. The AMS software version of the detector simulation and reconstruction used is v4.00/23/2 together with the GEANT version 3.21/13.

The protons were generated from a box of 3.9 m height centred on AMS according to the $\theta_{\rm p}$ and $\phi_{\rm p}$ distributions of an homogeneous and isotropic flux entering this box. The kinetic energy range of these protons lays between 0.265 GeV and 200 GeV.

The photons were generated from the same box but only on the upper side of the box and with discreet energies between 1 GeV and 300 GeV.

2.1 Proton Flux

The proton flux was measured by AMS01 at the altitude of approximately 380 km. In this note we used the measured proton flux at $\Theta_{\rm M} \geq 1$ from [4] and not the primary proton flux from [5] as used in the first note [1]. This results in slightly lower trigger rate.

2.2 Trigger Rate Calculation

The total trigger rate was calculated in bins of the proton kinetic energy $\rm E_p^{kin}$ using the proton sample:

$$\text{rate } (\mathrm{E_p^{kin}}) = \frac{\mathrm{N_p^{trig}(E_p^{kin})}}{\mathrm{N_p^{gen}(E_p^{kin})}} \times \mathrm{A_{box}} \times \Phi(\mathrm{E_p^{kin}}), \qquad (1)$$

where $\rm N_p^{trig}$ is the number of events triggered by the gamma trigger but not triggered by the standard ToF trigger and $\rm N_p^{gen}$ the number of generated events. The acceptance of the box is $\rm A_{box} = 6 \times \pi \times 3.9^2$ sr m^2 = 286.6 sr m^2. The definition of the $\rm E_p^{kin}$ bins and the corresponding integrated proton flux are given in table 2.

The rate can be decomposed as a function of the ECAL acceptance:

$$\text{rate } (E_p^{kin}) = \frac{N_p^{trig}(E_p^{kin})}{N_{ECAL}(E_p^{kin})} \times \frac{N_{ECAL}(E_p^{kin})}{N_p^{gen}(E_p^{kin})} \times A_{box} \times \Phi(E_p^{kin}). \quad (2)$$

N_{ECAL} is the number of events where the proton is crossing ECAL and

$$A_{ECAL}(E_p^{kin}) = \frac{N_{ECAL}(E_p^{kin})}{N_p^{gen}(E_p^{kin})} \times A_{box} \quad (3)$$

is the acceptance of the ECAL for protons with kinetic energies E_p^{kin}. The rejection factor of the stand-alone gamma trigger for protons entering ECAL is given by $N_{ECAL}(E_p^{kin})/N_p^{trig}(E_p^{kin})$.

This method is more precise than the one used in [1] as it takes into account the energy, θ_p and ϕ_p dependency of the ECAL acceptance. It also results in a lower trigger rate.

2.3 Photon Efficiency Calculation

The photon efficiency is calculated for photons which can be identified as such. That means they have to enter the ECAL and they also have to be in the ToF acceptance in order to be able to recognise them as neutral particles. To satisfy these two conditions the following selection is applied.

- Incident angle of the photon θ_γ lower than 20°
- X and Y impact coordinate of the photon track on the upper side of ECAL (Z= -147.2 cm) lower than 30.6 cm in absolute value.
- X and Y impact coordinate of the photon track on the ToF 1 and 2 (Z= +55 cm and Z= -55 cm) lower than 70 cm in absolute value.

The stand-alone gamma trigger is foreseen to trigger only on gamma reaching the ECAL therefore converted gammas were rejected from the sample. The photon efficiency ε_γ is then:

$$\varepsilon_\gamma = \frac{N_\gamma^{trig}}{N_\gamma} \quad (4)$$

where N_γ represents the number of non converted photons and N_γ^{trig} the number of photons which have passed the trigger.

2.4 Trigger Algorithm

The trigger algorithm presented in [1] was optimised for energies in ECAL larger than 8 GeV. The 9 layers were used and a threshold of 100 MeV was finally chosen to be applied on each dynode for the determination of $N_X + N_Y$. To have a trigger already efficient for gamma energies above 3 GeV the total energy threshold is decreased to 2 GeV which results in a dramatic increase of the trigger rate. To keep the trigger rate below 50 Hz deepened studies were necessary. They have led to the following.

- Two additional steps in E_{tot} are defined for $E_{tot} < 8$ GeV.
- The first layer from the top of ECAL was removed from the trigger algorithm (columns of 4 PMTs in X and Y). This does not affect the photon efficiency as for photons very little energy is deposited in the first layer.
- The cuts on $N_X + N_Y$ were optimised for two different values of the column threshold, 100 MeV for scenario 1 and 90 MeV for scenario 2. Figure 2 shows the total energy deposit in ECAL versus $N_X + N_Y$ for photons and protons. The larger contribution of the proton rate corresponds to protons giving less than 4 GeV in the ECAL.

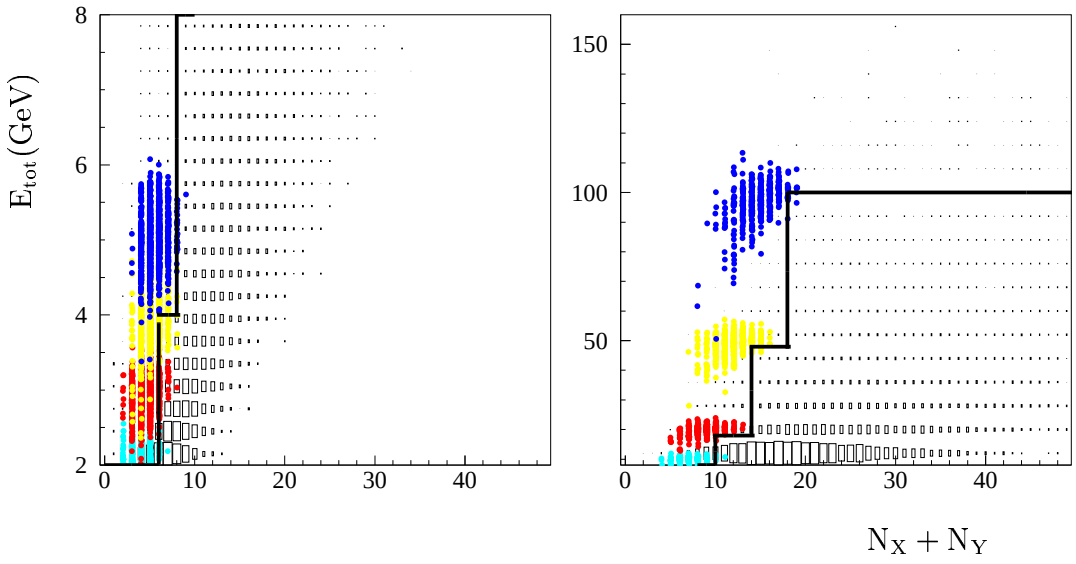

Figure 2: Total energy deposit in ECAL versus $N_X + N_Y$ in case of scenario 2 for photons (E_γ =2,3,4,5,10,20,50,100 GeV) represented by points and protons (E_p^{kin} from 0.5 GeV to 200 GeV) represented by rectangle with surface proportional to the rate. On the left and right plot the larger rectangles corresponds to 16.7 Hz and 2.1 Hz respectively.

- For E_{tot} between 2 GeV and 4 GeV we require less than three blocks of columns: $N_{block} < 3$. A block is defined as one or more adjacent columns above threshold delimited by at least one empty column on both sides. N_{block} is the number of blocks in X and Y separately. The cut on N_{block} allows to suppress side going protons at low E_{tot} for which the width cut is not so powerful anymore. These protons fire non consecutive columns or groups of columns whereas a photon shower results in only one group of columns in each direction.

Final cuts after optimisation are summarised in table 1 for the two scenarios.

Energy range	Trigger algorithm		
	defined in [1]	scenario 1	scenario 2
2 GeV $< E_{tot} <$ 4 GeV		$N_X + N_Y < 6$ $N_{block} < 3$	$N_X + N_Y < 7$ $N_{block} < 3$
4 GeV $< E_{tot} <$ 8 GeV		$N_X + N_Y < 8$	$N_X + N_Y < 9$
8 GeV $< E_{tot} <$ 18 GeV	$N_X + N_Y < 10$	$N_X + N_Y < 10$	$N_X + N_Y < 11$
18 GeV $< E_{tot} <$ 48 GeV	$N_X + N_Y < 13$	$N_X + N_Y < 14$	$N_X + N_Y < 15$
48 GeV $< E_{tot} <$ 100 GeV	$N_X + N_Y < 16$	$N_X + N_Y < 19$	$N_X + N_Y < 19$

Table 1: Trigger algorithm defined in [1]: dynode threshold of 100 MeV, columns of 4 PMTs in X and 5 PMTs in Y. Upgraded algorithms allowing to lower the E_{tot} threshold to 2 GeV: column threshold of 100 MeV (scenario 1) or 90 MeV (scenario 2), columns of 4 PMTs in X and Y.

2.5 Results

In this section we present the results of the trigger simulation. In a first part, the trigger rate at the level 0 (fast trigger) and level 1 caused by cosmic protons are determined. In second part, we give the corresponding gamma efficiencies for gamma energies between 1 GeV and 300 GeV.

Trigger Rate

At the level 0 the only condition is a total energy deposited in ECAL larger than 2 GeV. This corresponds to a rate of 410 Hz which stays safely lower than the maximum allowed rate of 1 kHz.

		scenario 1		scenario 2	
E_p^{kin} GeV	Flux Hz sr^{-1}m^{-2}	rate Hz	acceptance srm^2	rate Hz	acceptance srm^2
0.265 - 0.5	315.4	0.08	0.27	0.08	0.27
0.5 - 1.5	969.5	0.40	0.41	0.27	0.28
1.5 - 2.5	443.6	3.22	7.26	4.03	9.08
2.5 - 3.5	238.8	3.88	16.26	4.76	19.95
3.5 - 4.5	143.6	4.43	30.82	5.17	36.04
4.5 - 5.5	92.5	2.95	31.89	3.75	40.59
5.5 - 6.5	62.9	1.75	27.88	3.17	50.33
6.5 - 7.5	44.6	1.78	39.80	2.40	53.84
7.5 - 8.5	32.7	1.40	42.67	2.33	71.11
8.5 - 9.5	24.7	0.87	35.27	1.16	47.03
9.5 - 10.5	19.1	1.06	55.60	1.48	77.41
10.5 - 11.5	15.0	0.91	60.71	1.27	84.52
11.5 - 12.5	12.0	0.51	42.18	0.71	58.80
12.5 - 13.5	9.8	0.53	54.28	0.76	77.94
13.5 - 14.5	8.1	0.52	64.15	0.62	76.08
14.5 - 15.5	6.7	0.54	81.19	0.61	92.23
15.5 - 16.5	5.7	0.41	72.76	0.57	99.83
16.5 - 17.5	4.8	0.27	55.56	0.38	78.86
17.5 - 18.5	4.1	0.19	46.85	0.24	58.10
18.5 - 19.5	3.6	0.20	55.81	0.28	79.74
19.5 - 20.5	3.1	0.17	54.43	0.25	81.65
20.5 - 25.3	10.5	0.64	61.38	0.87	82.67
25.3 - 31.2	7.0	0.49	70.03	0.65	93.70
31.2 - 38.4	5.5	0.45	82.05	0.58	106.8
38.4 - 47.3	4.2	0.39	92.73	0.46	110.4
47.3 - 58.2	3.1	0.36	115.9	0.43	138.5
58.2 - 71.5	2.0	0.22	112.5	0.26	133.7
71.5 - 87.8	1.3	0.16	122.3	0.19	150.9
87.8 - 108.8	0.89	0.12	129.5	0.13	150.2
108.8 - 132.3	0.64	0.10	163.5	0.11	177.3
132.3 - 162.3	0.42	0.08	194.1	0.09	207.0
162.3 - 199.1	0.31	0.08	257.3	0.08	276.0
TOTAL	2495.5	29.2	11.69	38.2	15.30

Table 2: Cosmic proton flux from [4], trigger rate and acceptance for the two scenarios in E_p^{kin} bins.

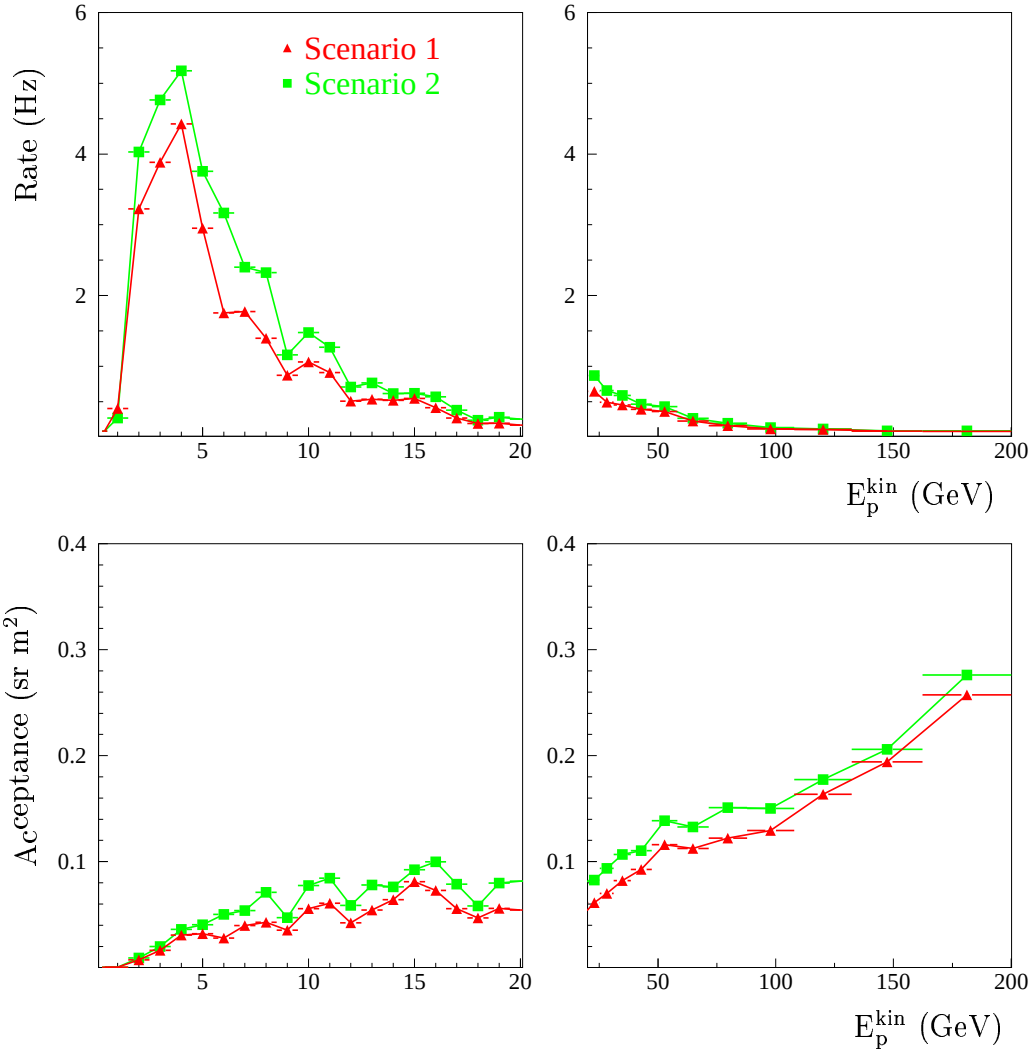

Figure 3: Trigger rate from cosmic protons and trigger acceptance as a function of proton kinetic energy. The squares and triangles represent the trigger results in case of scenarios 1 and 2 respectively.

For the final decision the rate and acceptance (rate/Φ) in E_p^{kin} bins are presented in table 2 and figure 3 for the two different scenarios. A total rate of 29 Hz is found when scenario 1 is applied and 38 Hz in case of scenario 2. The step in the rate at $E_{tot} > 20$ GeV corresponds to larger bins sizes. The main contribution to the rate comes from protons with kinetic energies lower than 8 GeV.

In figure 4 the proton rate is shown as a function of E_{tot}, ϕ_p, θ_p and $\cos(\theta_p)$. In case of scenario 2, 85 % of the total rate comes from events with a total energy in the ECAl lower than 5 GeV, 60 % from events with a total energy in the

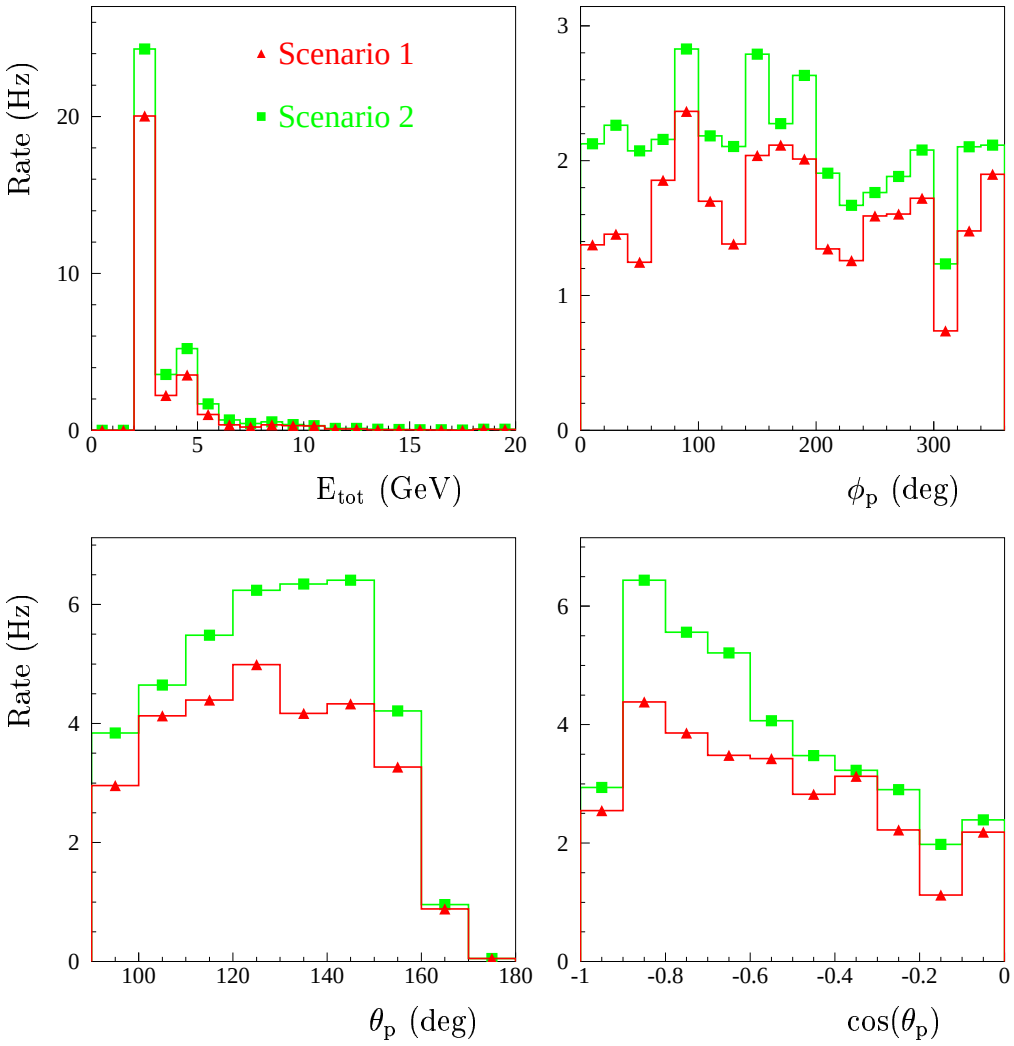

Figure 4: Trigger rate from cosmic protons as a function of E_{tot}, ϕ_p, θ_p, cos(θ_p). The triangles and squares represent the trigger results in case of scenarios 1 and 2 respectively.

ECAl lower than 3 GeV. The θ_p distribution shows that horizontal protons which contribute mainly to the high rate are efficiently rejected. The rate distribution is nearly flat in ϕ_p.

The proton rejection factor is shown in figure 5 as a function of E_{tot}, ϕ_p, θ_p, cos(θ_p). The effect of the $N_X + N_Y$ cut in E_{tot} steps can be observed in the rejection factor as a function of E_{tot}. The θ_p distribution shows a large rejection factor at $\theta_p > 60°$ which corresponds to the protons accepted by the ToF trigger (not considered as selected by the photon trigger, see subsection 2.2).

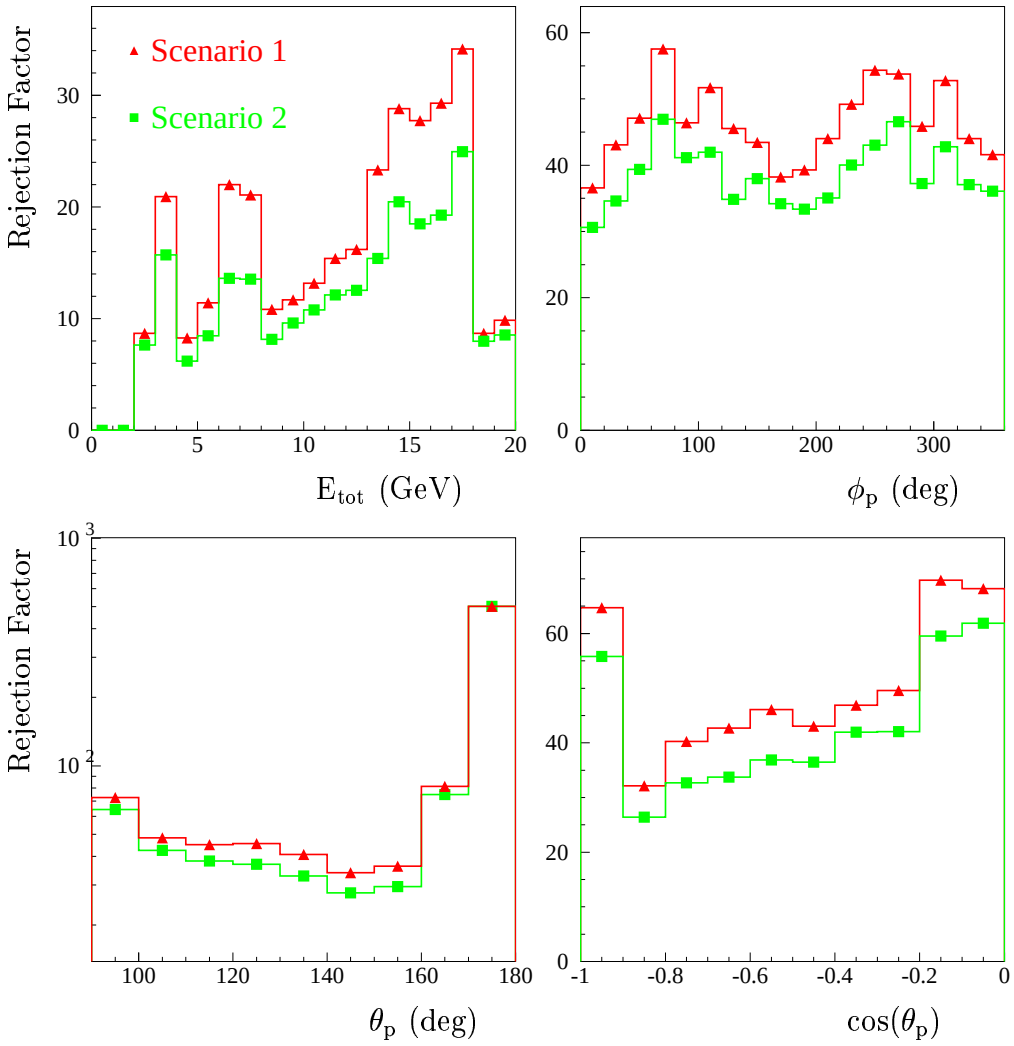

Figure 5: Trigger rejection factor for cosmic protons as a function of E_{tot}, ϕ_p, θ_p, $\cos(\theta_p)$. The triangles and squares represent the trigger results in case of scenarios 1 and 2 respectively.

The efficiency of the photon trigger for horizontal protons is demonstrated by an increase of the rejection factor for decreasing θ_p. The ϕ_p rejection factor seems to be higher in the Y direction ($\phi_p \approx 90°$ or $270°$) than in the X direction ($\phi_p \approx 0°$ or $180°$) which could be the consequence of the magnetic field.

Photon Efficiency

The trigger efficiency for gammas between 1 GeV and 300 GeV is given in table 3 for two ranges of the gamma incident angle and for the two scenarios. For scenario 2, a photon efficiency of 96.4 % is already reached at photon energies of

3 GeV where scenarios 1 gives only 90.9 %. We have seen that the trigger rate for scenario 2 is 38 Hz instead of 29 Hz for scenario 1 which stays however quite lower than the maximum rate allowed. Scenario 2 provides therefore the more efficient trigger. In the following, we will present the robustness study in case of scenario 2.

E_γ	ε_γ - scenario 1		ε_γ - scenario 2	
(GeV)	$0° < \theta_\gamma < 10°$	$10° < \theta_\gamma < 20°$	$0° < \theta_\gamma < 10°$	$10° < \theta_\gamma < 20°$
1	0 %	0 %	0 %	0 %
2	44 %	41 %	43 %	42 %
3	94 %	89 %	97 %	96 %
4	95 %	89 %	98 %	97 %
5	100 %	99 %	100 %	100 %
10	100 %	99 %	100 %	100 %
20	99 %	99 %	100 %	100 %
50	99 %	99 %	100 %	100 %
100	99 %	100 %	99 %	100 %
300	100 %	99 %	100 %	99 %

Table 3: Photon efficiencies in % for the two algorithms.

2.6 Robustness

In this section the robustness of the stand-alone gamma trigger is presented using the scenario 2 for the trigger algorithm.

Dynode Smearing

First we have checked the trigger stability with respect to a more realistic answer of the dynode signals. Indeed, in the simulation version used to produce the photon and proton samples no dynode signals are available. A dynode signal is simply taken to be the sum of the four corresponding anodes. This results in a too good total energy resolution reconstructed with the dynode signals. In order to reach the energy resolution measured with the test beam data of July 2002:

$$\frac{\sigma(E_{tot})}{E_{tot}} = \frac{16\%}{\sqrt{E_{tot}(GeV)}} \oplus 4\%, \tag{5}$$

the individual anode signals were additionally smeared with a function depending on the particle momentum. The effect on the trigger rate and efficiency is negligible (see figure 6).

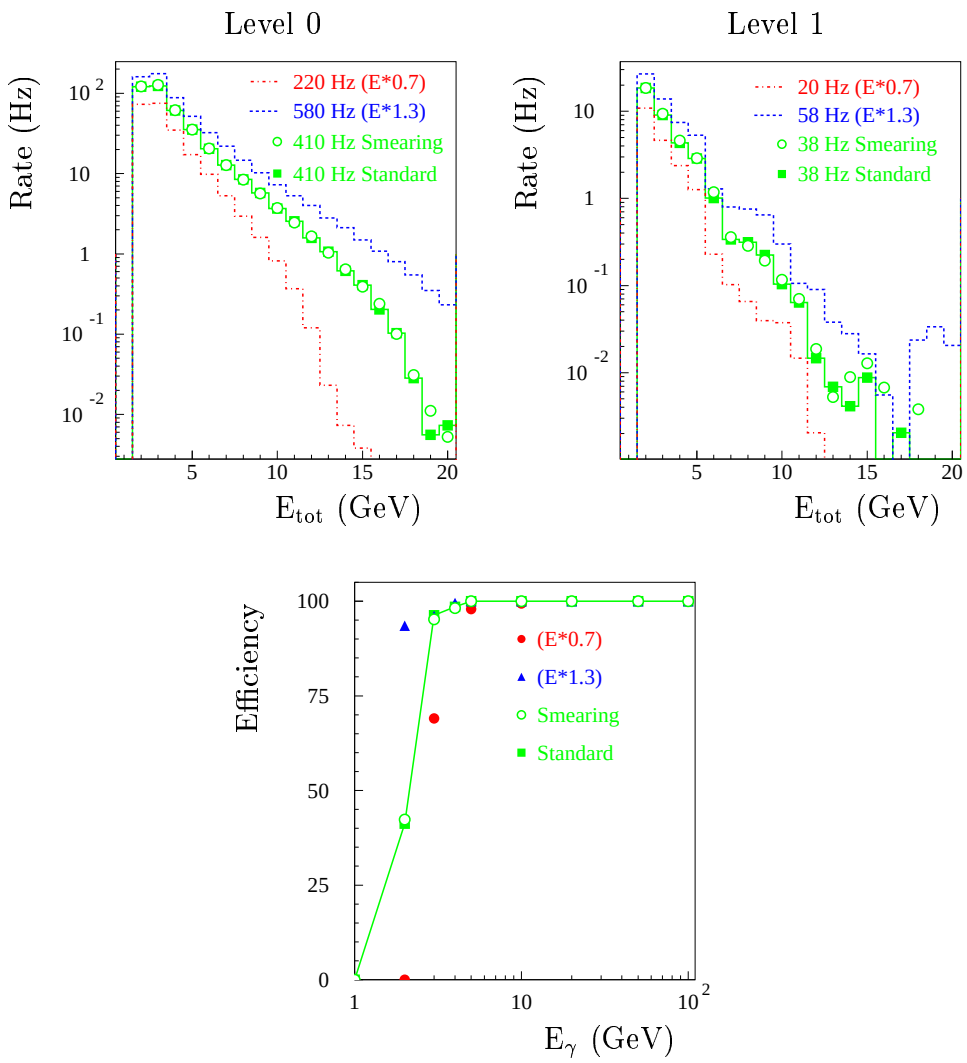

Figure 6: Level 0 and level 1 rate as a function of E_{tot} (GeV) and efficiency as a function of E_γ for scenario 2 (squares), after a smearing of the dynode signals (open circles), after a systematic gain shift of +30 % (dashed line and triangles) or -30 % (doted-dashed line and full circles).

Systematic Gain Shift

The trigger performance was subject to systematic gain shifts of +30 % or -30 %. This results in trigger rate variations from 220 Hz to 580 Hz at the level 0 and 20 Hz to 56 Hz at the level 1. The trigger efficiency is only affected for $E_\gamma < 4$GeV. An increase of 30 % allows to trigger 3 GeV gammas with 92 % efficiency with a rate of 56 Hz which stays acceptable. On the other hand, a decrease of the gain is more dangerous as it lowers the trigger efficiency. This can be however mitigated by decreasing the first energy threshold to 1.4 GeV. In this case the efficiency at 3 GeV is 99.4 % and a rate of 77 Hz.

Defective Dynode Channels

One, five or ten defective dynode trigger lines were implemented using 20 different configurations. To check the robustness of our algorithm and of the algorithm proposed by the INFN-Sezione di Pisa the configurations were chosen in common. Most of them are random configurations plus a couple of configurations specially destructive for one or the other algorithm (problematic channels concentrated in columns or in planes). Three different cases of problems were studied:

- dead PMTs which means no dynode answer,
- gain shift of +30 % or - 30 %,
- gain with a factor 10 higher (could come from faulty amplifiers, HV failure).

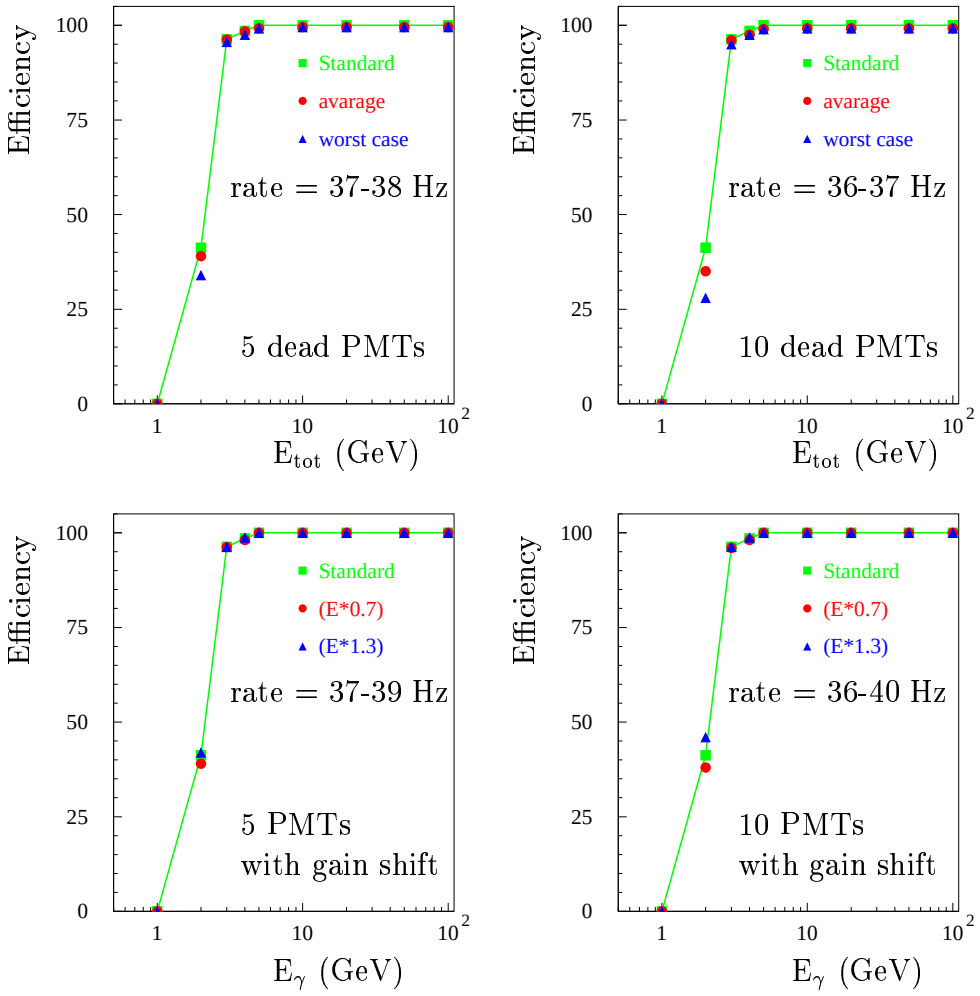

Figure 7: Photon efficiency as a function of E_γ for the scenario 2 (squares), in case of 5 (left upper plot) or 10 (right upper plot) dead PMTs (full circles for average of all configurations, triangles for the worst case with respect to ε_γ) and in case of 5 (left lower plot) or 10 (right lower plot) PMTs with gain shift of +30 % (triangles) and -30 % (full circles).

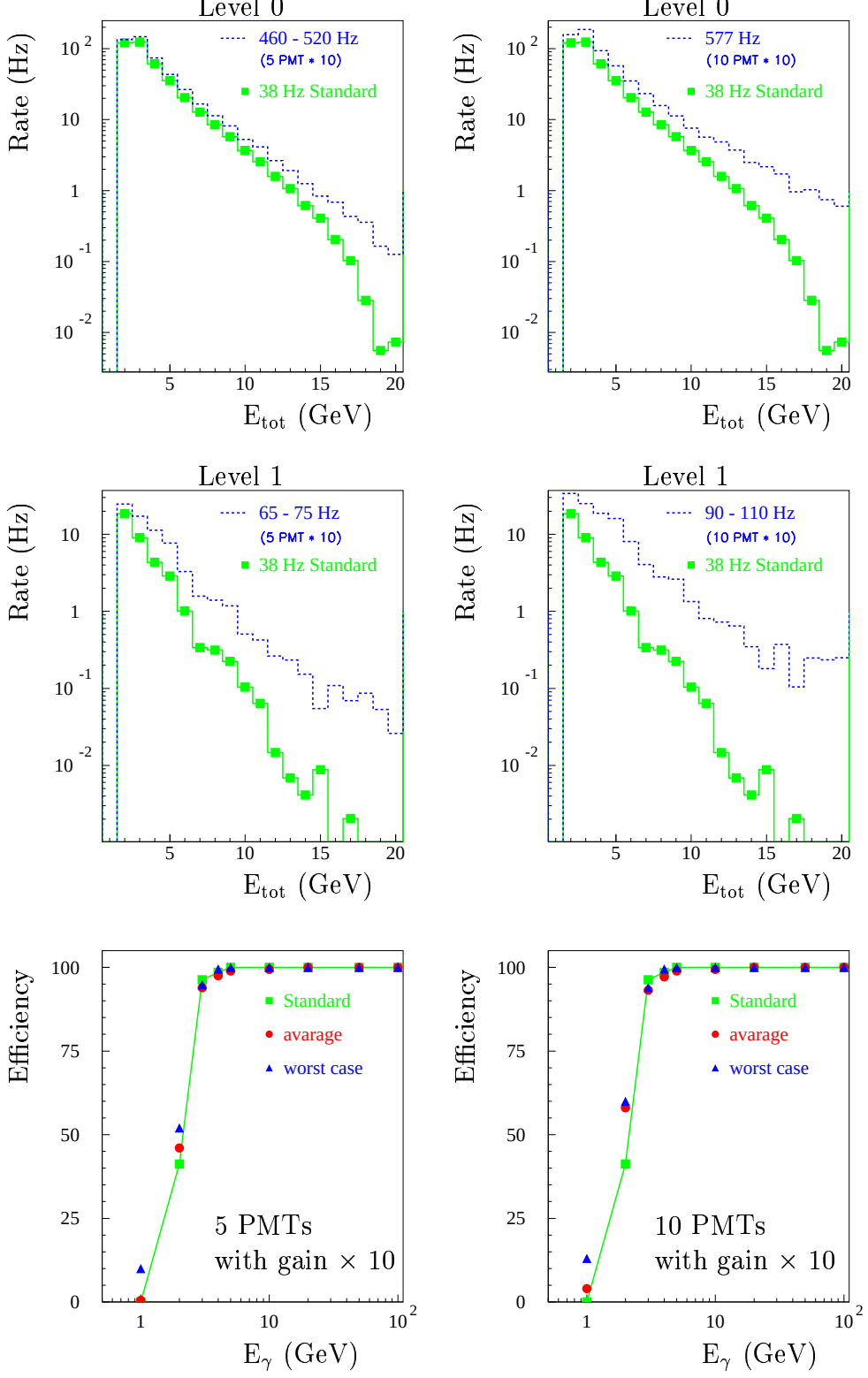

Figure 8: Level 0 and Level 1 rate as a function of E_{tot} (GeV) and efficiency as a function of E_γ for scenario 2 (squares), in case of 5 (left plots) or 10 (right plots) PMTs with gain a factor 10 higher (dashed line and full circles for average of all configurations, triangles for the worst case with respect to trigger rate).

The rate and efficiency is not changed when only one dynode signal is problematic.

The changes in the trigger rate and efficiency are summarised in figure 7 and figure 8. For photons with energies equal or above 3 GeV the trigger efficiency is stable against the three different kind of problems whether they affect 5 or 10 PMTs. This is also the case for the trigger rate except when the gain is a factor 10 higher where the level 1 rate can reach 110 Hz.

3 Technical Project (Implementation)

3.1 Introduction

The AMS trigger timing requirements are summarised in figure 9. The consequence for the electronics of the ECAL trigger is to provide:

- the analog sum corresponding to the total deposited energy in the ECAL in less than 200 ns,
- the final decision based on 5 different thresholds of the analog sum and on the number of hit columns (WIDTH) in less than 900 ns.

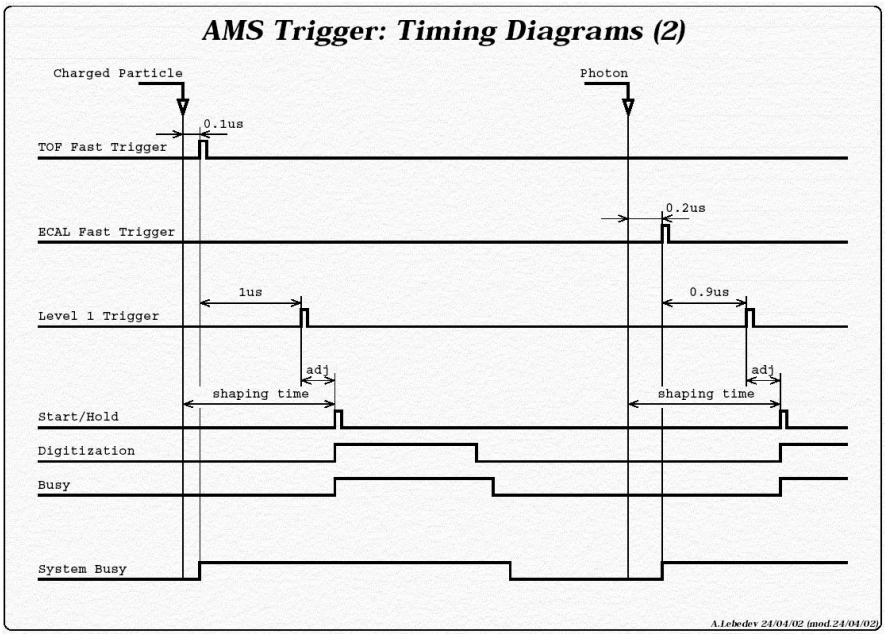

Figure 9: AMS timing requirements on trigger signals. One the left side for a charged particle crossing the detector and on the right side for a photon.

In general, the considered analog signals have small amplitudes. The analog part of the trigger electronics has therefore to be as close as possible to the PMT and its read-out electronics in order to minimise signal attenuation due to cable length. As a consequence the trigger electronics is planed to be on the EIB board whose primary function is to collect the output signals of 4 or 5 PMTs and to transmit them to the EDR board situated in the ECAL crates. Like for the standard signals, the trigger signals (resulting from 6 different thresholds for the analog sum and one column threshold for the width) are converted in LVDS signals and transit through the EDR board. They are then numerically treated in a dedicated board named ETRG (for Ecal TRiGger). The EDR boards and the ETRG board are situated in one of the two crates fixed to the ECAL supporting structure. In this configuration only digital signals travel between the ECAL and the crates. The LVDS technology was chosen to obtain the most reliable data transfer.

The main difficulty with respect to the electronics is to obtain the analog sum in less than 200 ns together with a low power consumption of the system (<15 W). In this part of the note the emphasis is put on the structure of the trigger electronics, on its consumption and on the estimation of the delays for the different stages (see also [6]).

3.2 Dynode Signal

During the test beam phase in July 2002 it was successfully demonstrated that the dynode read-out does not disturb the anode output. The same should be reached for the trigger electronics.

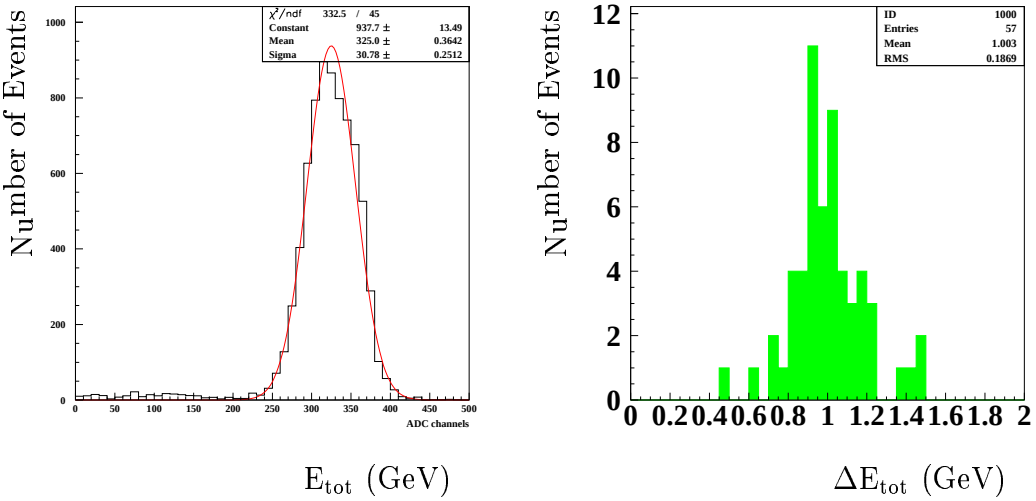

Figure 10: Total energy distribution in ADC channels using the dynode outputs for a 10 GeV electron beam and dispersion of the dynode energy sum from electron equalisation runs.

The results of the test beam are summarised in figures 10 and 11. For a total deposited energy of 10 GeV, 325 ADC channels are summed for the whole ECAL (see figure 10). The ADC used is a 12 bits ADC with 4096 steps between 0V to 3V which gives:

$$1 \text{ GeV deposited energy} <=> 23 \text{ mV dynode signal.} \quad (6)$$

This information is necessary to determine the gain for the different steps and the thresholds of the comparators. Moreover, a fairly good energy linearity and resolution was observed together with a low dispersion of the raw dynode outputs which has demonstrated that the dynode signals are sufficient for building the trigger system.

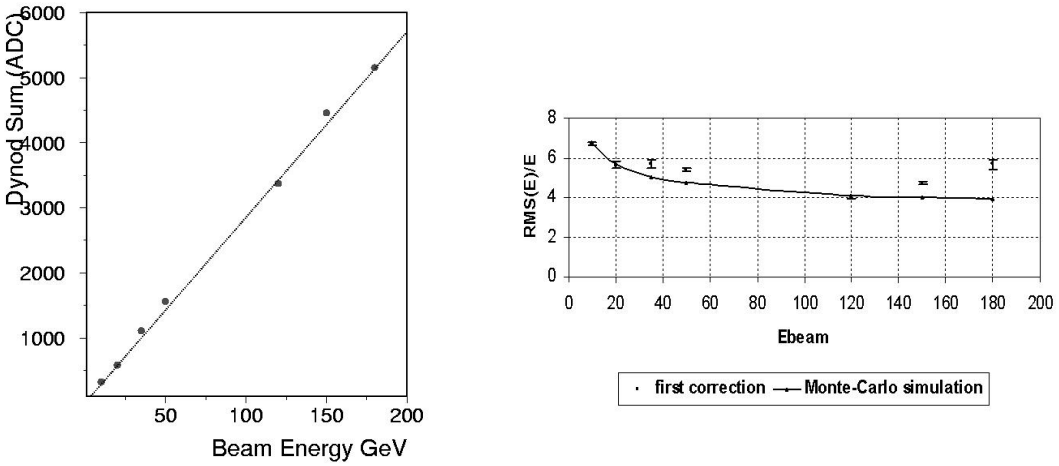

Figure 11: Energy resolution and linearity using the dynode signals obtained with the test beam data of July 2002.

3.3 Architecture Description

Analog Sum Circuit

The synoptic of the analog sum circuit is represented in figure 12. The analog sum circuit consists of 6 stages with the 2 first stages in common with the WIDTH circuit.

- The dynode load is a RC network in common for the trigger line and the read-out line (front end shaping circuit + ADC) with a time constant of 470 pF$\times$2.2 kΩ = 1 μs. For the trigger line, the first component is a follower in order to present an infinite impedance to the dynode output. This prevents perturbation in the front end shaping circuit.
- The second stage is an adder of the 4 dynode signals for one column.

- The 18 columns of one face are summed with an 18-input adder.
- The 4 faces are summed with a 4-input adder plus an inverter in order to obtain a positive signal with a linear behaviour from 0 V to 1.8 V.
- In the next stage the signal is compared to the 6 thresholds. The output of each comparator is a CMOS 0/+3V compatible signal (active high logic).
- At the last stage 6 D flip-flops (edge-triggered D-latches) for each threshold lines store the output of the comparators. These informations are converted in LVDS format by a LVDS driver and are sent to the ETRG board via 6 twisted pairs LVDS wires.

For the analog sum, the different adder outputs have to be weighted by adjusting the gain in order to reach approximatively 2 V at the final output for the higher energy threshold of 100 GeV.

The gains were adjusted considering a 100 GeV photon with energy distributed over 8 columns with 2 columns per side. This represents 12.5 GeV per hit column which corresponds to a column signal of 250 mV (20 mV for 1 GeV). In this case the weighting factors have to be 1 since there are already at the input 8×250 mV = 2 V. It is important that the system stays linear up to this value. Unfortunately the imposed power supply for the amplifier LMH664x of +3V/-2V leads to saturation starting around 1.8 V (negative signals) which will be the higher threshold possible.

The comparator thresholds are chosen according to the energy thresholds defined in section 2.4 (except for the higher threshold):

40 mV for 2 GeV,
80 mV for 4 GeV,
160 mV for 8 GeV,
400 mV for 18 GeV,
1 V for 48 GeV,
1.8 V for 90 GeV.

In order to have 1.8 V at the output of the analog sum corresponding to 100 GeV the loads of the adders have to be adjusted to obtain weighting factors slightly below 1.

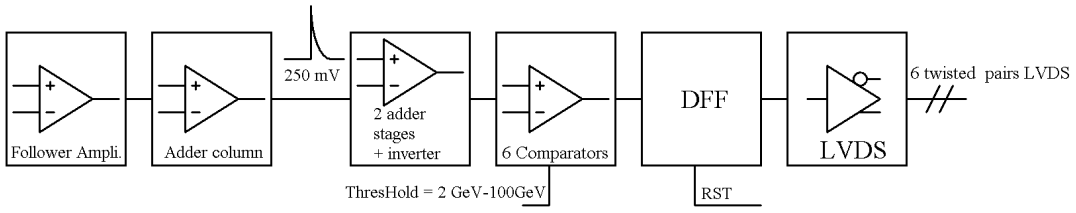

Figure 12: Synoptic of the analog sum circuit.

WIDTH Circuit

After the first two stages in common with the analog sum circuit, an amplification is needed in order to apply a column threshold corresponding to 100 MeV (see figure 13). At the dynode output the signal amounts 2 mV for 100 MeV energy deposited (see section) while the comparator shows good performances for thresholds greater than 15 mV to 20 mV. Therefore an Op Amp with a gain of 10 is necessary. Like for the analog sum the output state of each column comparator is stored in memory with a D flip-flop and converted in LVDS format to be sent to the ETRG board.

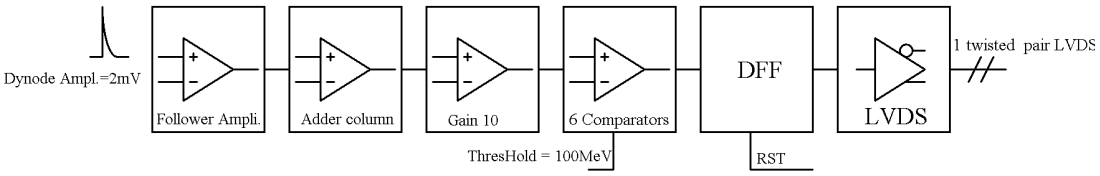

Figure 13: Synoptic of the transverse WIDTH circuit.

Remarks

The schematic of the analog part of the trigger electronics for the analog sum and the WIDTH is shown in figure 14. With this architecture a total number of 84 comparators and 480 amplifiers is reached taking into account redundancy (see section 3.4.3). Special care has been taken to avoid problems of noisy channels. Indeed analog switches (DG419 from Vishay Siliconix) are foreseen in order to disconnect problematic dynodes which could be responsible for inopportune triggering of the D flip-flop (see figure 15).

3.4 Prototype Performances

The active component performances as well as the strategies for the redundancy has allowed to finalise the prototype and to determine the power consumption. The choice of the components was essentially based on the rapidity to consumption ratio and the redundancy was thought in order to limit the amount of additional components.

3.4.1 Component Choice: the Amplifier

The chosen amplifier chips are the LMH6642/43/44 from National Semiconductor. The LMH664x family allows a flexible implementation as it corresponds to one, two or four amplifiers per chip.

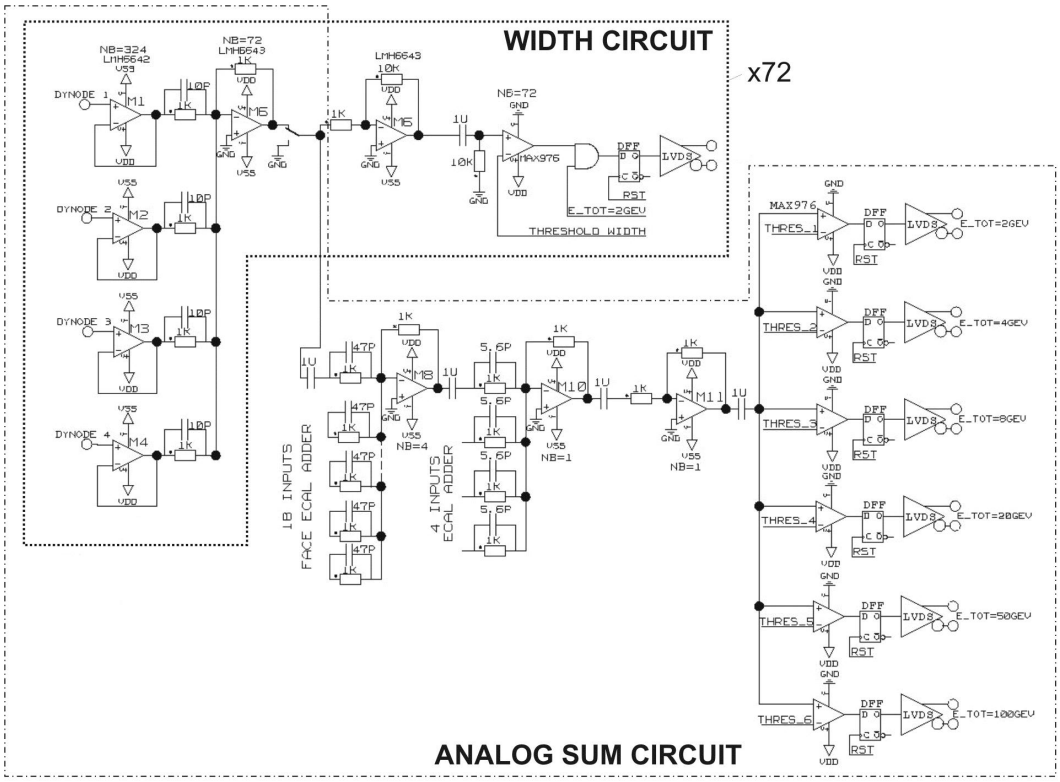

Figure 14: Schematic of the analog part of the ECAL trigger electronics: the analog sum (with 6 thresholds) and the WIDTH (with one threshold per column).

The characteristics of the operational amplifier (Op Amp) are given in table 4. The choice of the Op Amp was performed in order to restrict two effects. Firstly, a fast answer of the Op Amp is required since 5 Op Amps are cascaded to provide the analog sum. Secondly, it is fairly important to minimise the deformation of the signal, so a high slew rate (V/μs) is desired.

Parameters	Typical values	Units
Voltage Supply	3 to 12.8	V
Input Bias Current	-1.5	μA
Current Supply	2.7	mA
Slew Rate	130	V/μs
Bandwidth	130	MHz
Output Current	$\pm$ 75	mA

Table 4: Characteristics of the LMH6642/43/44 amplifier.

The chosen Op Amp works for a +3/-2V supply. Its output is Rail-to-Rail which means it only presents a small voltage drop with respect to the voltage supply. This Op Amp still has to be space qualified in the sens that it should resist to a high level of radiations and withstands vibrations and thermal variations.

3.4.2 Component Choice: the Comparator

The chosen comparator type is MAX976 from Maxim, its characteristics are given in table 5.

As for the amplifier the comparator has to have a fast answer for all required thresholds. It should work in 0/+3V and be compatible with CMOS input of the D flip-flop.

The need of a small threshold comparator involves two risks:

- The delay of the comparator is a function of the threshold value and of the input signal amplitude. For example, with a 15 mV threshold the delay can reach 100 ns for a 20 mV signal.
- The minimal threshold value is limited by the offset at the input. Working close to the offset input level can lead to a non commutation of the comparator because of its internal hysteresis.

Parameters	Typical values	Units
Propagation Delay	3 to 12.8	ns
Voltage Supply	2.5 to 5.5	V
Current Supply	225	μA
Rise/Fall Time	1.6	ns
Input Offset Voltage	$\pm$ 3	mV

Table 5: Characteristics of the MAX976 comparator.

3.4.3 Redundancy

The redundancy of the trigger chain starts after the dynode sum of each column and only the chain of the analog sum is doubled (see figure 15). This allows to limit both the number of components and the power consumption, together with keeping redundancy of the vital functions needed for the realisation of the analog sum. Table 6 summarises the number of components with and without redundancy.

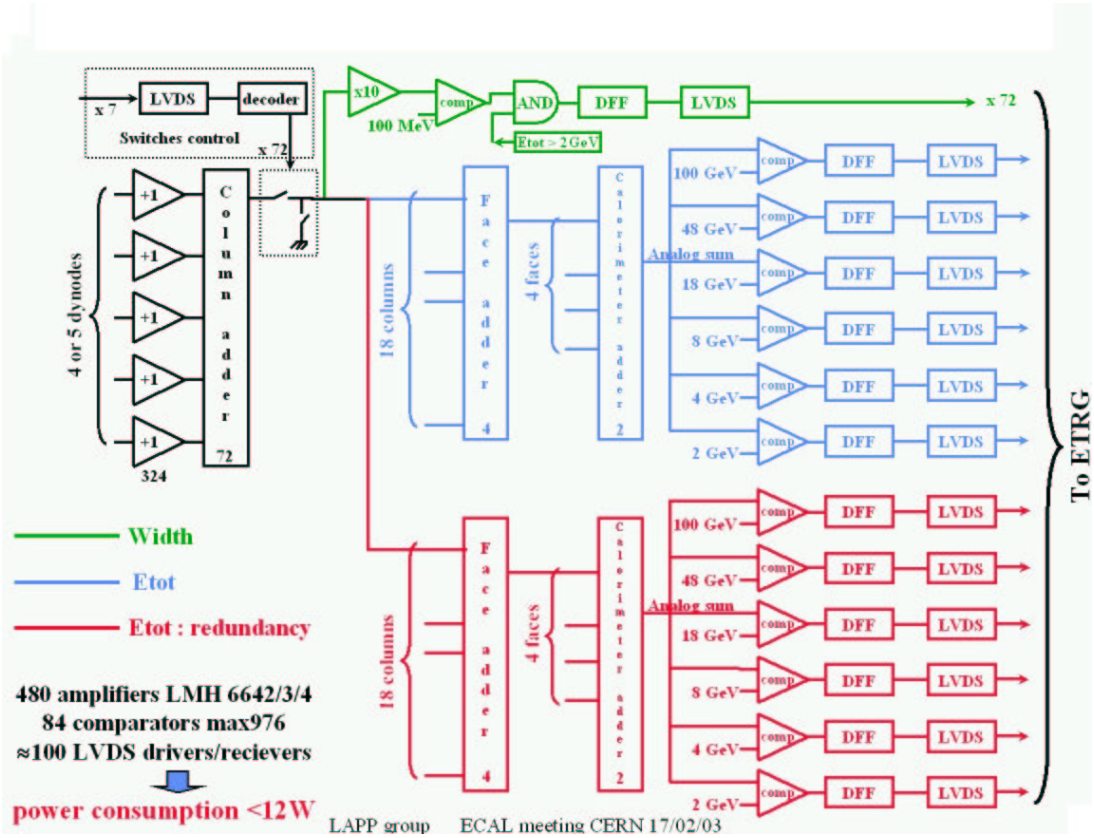

Figure 15: Main synoptic of the analog part of the ECAL trigger electronics with redundancy of the analog sum.

Localisation	Number of Components	Number of Components with Redundancy
Face Adder	4	8
ECAL Adder	1	2
ECAL Inverter	1	2
Comparator	6	12
D flip-flop	6	12
LVDS driver	6	12

Table 6: Number of components without and with redundancy.

3.4.4 Power Consumption

The power consumption was determined including redundancy of the analog sum as described in section 3.4.3. Table 7 gives typical values for the different components and results in a total power consumption of 8.3 W.

Component	Individual Power Consumption	Number of Components (with Redundancy)	Power Consumption
LMH664x	13.5 mW	480	6.5 W
MAX976	825 μW	84	70 mW
LVDS driver	16.5 mW	100	1.7 W
Total		664	8.3 W

Table 7: Summary of the trigger power consumption.

3.4.5 Reset

The stand-alone gamma trigger will allow the read-out of the full AMS raw data when a gamma crosses the detector. However, in order not to have all column lines getting progressively fired one after the other because of the constant crossing of cosmic rays of all types, a reset of the column D flip-flop is necessary after each particle crossing.

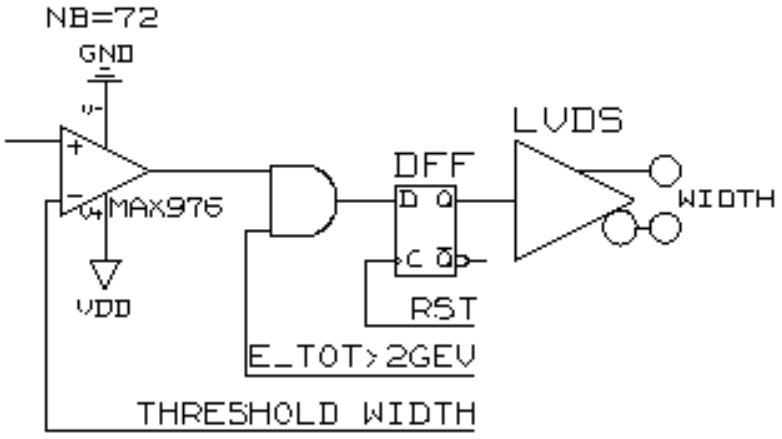

Figure 16: Schematic for the end of the WIDTH trigger line. The comparator output is sent to the D flip-flop only if the analog sum is greater than 2 GeV.

The easiest solution is to implement an auto-reset of the D flip-flop. A more robust solution is to validate the output of the column comparator only if the analog sum is above the first energy threshold. This is done by adding a AND gate between the column comparator and the D flip-flop (see figure 16). When the energy threshold is above 2 GeV all D flip-flops are reseted from the ETRG board right after the level 1 decision.

3.5 Test Bench and Results

The tests performed to validate the trigger proposal were based on timing measurements of the analog parts of the trigger system. Indeed the critical part is to get the analog sum in less than 200 ns (fast trigger). The information of the WIDTH is needed to compute the level 1 answer and brings a significant delay compared to the digital signal processing. To reach the best performances we have carefully controlled the contribution of each component to the delay and to the signal deformation.

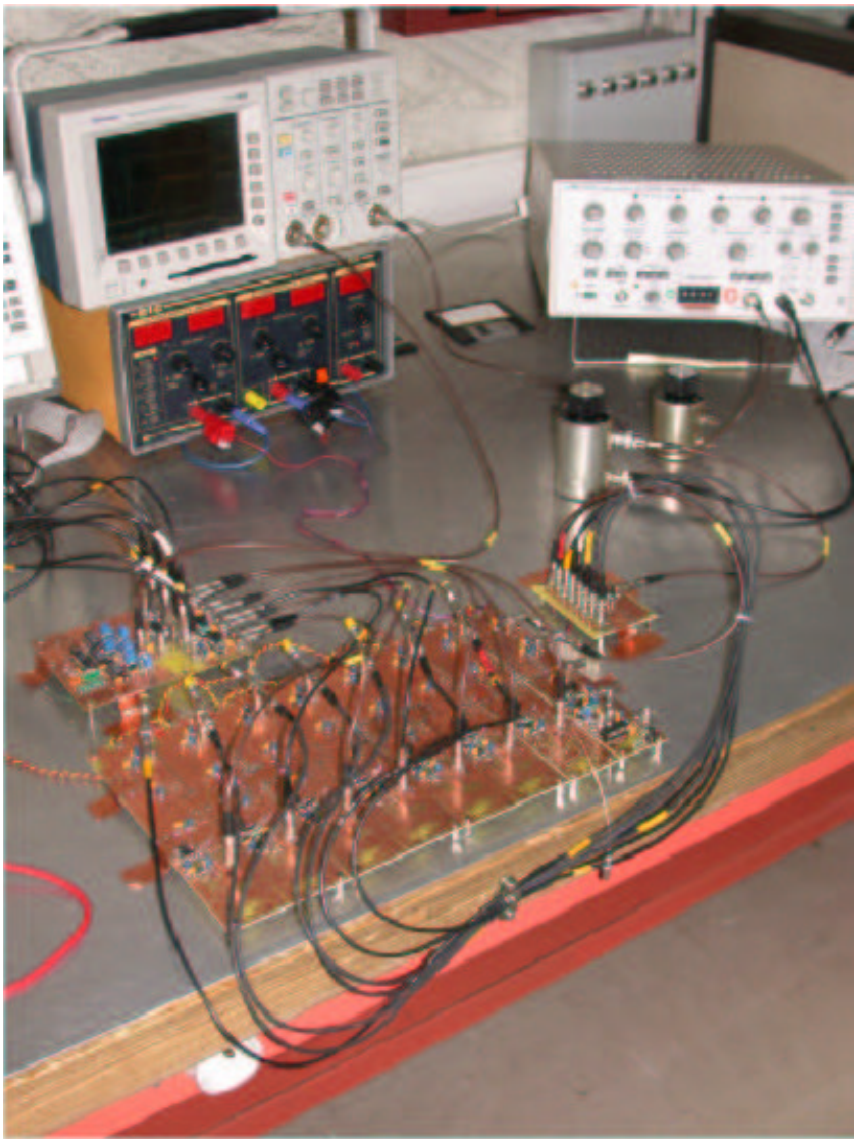

Figure 17: Test bench.

The test bench we have built for this purpose is shown in figure 17. The cable lengths were chosen to reproduce the situation around the ECAL: 30 cm cable length between the column adder and the face adder, 3 m cable length between the face adder and the ECAL adder.

Analog Signal Injection

The input signal were not the one from several PMTs but were faked by an equivalent input circuit. This circuit must deliver 8 positive signals with fast rise time (about 10 ns) and 1 μs falling time which are standard dynode signals.

For a single signal the cable used to bring it to the trigger circuit must be terminated at both ends with 50 Ω. This results in an input signal of the trigger circuit with half the amplitude of the generated one. With an amplifier, set to a gain of 2 and situated before the first matching resistor, a one to one ratio is obtained. In our case the signal is split into 8 lines. Therefore the matching resistor on the injection board should be realised with one resistance R1 in common for the 8 lines and 8 resistances R2 for each line. The resistance R1 and R2 for n lines are given by

$$\frac{\mathrm{R2} + 50\,\Omega}{n} + R1 = 50\,\Omega. \tag{7}$$

With R1 = R2 = R:

$$R = \frac{\mathrm{n} - 1}{\mathrm{n} + 1} \times 50\,\Omega. \tag{8}$$

For n=8 the resistances should amount 38.8 Ω. The schematic of the input circuit is shown in figure 18.

Analog Sum Delay

The analog sum circuits allows to obtain a signal proportional to the total energy deposited by a particle in the ECAL. It represents a summation of 288 inputs (4 PMTs $\times$ 18 columns $\times$ 4 faces). This is performed by implementing 3 stages of summation and 5 Op Amp (as described in section 3.3 and shown in figure 14), each contributing to the total delay of the circuit. The delay differs from one stage to the other and depends on the gain at the working point. At the end of the summation the delay induced by the comparator depends on its threshold and on the amplitude of the input signal.

The summation performed is far from trivial. More especially when not all inputs are active, the higher the number of inputs summed in one stage the higher the deformation of the signal is. Indeed, the front edge of the signal gets smoother. The critical point is situated at the summation of the 18 columns. At this stage the resistors of each input were chosen to amount 1 kΩ in order to obtain a non scaled sum of all inputs at the output of the adder. However, an adder with 18 inputs introduces a short equivalent resistor which results in a

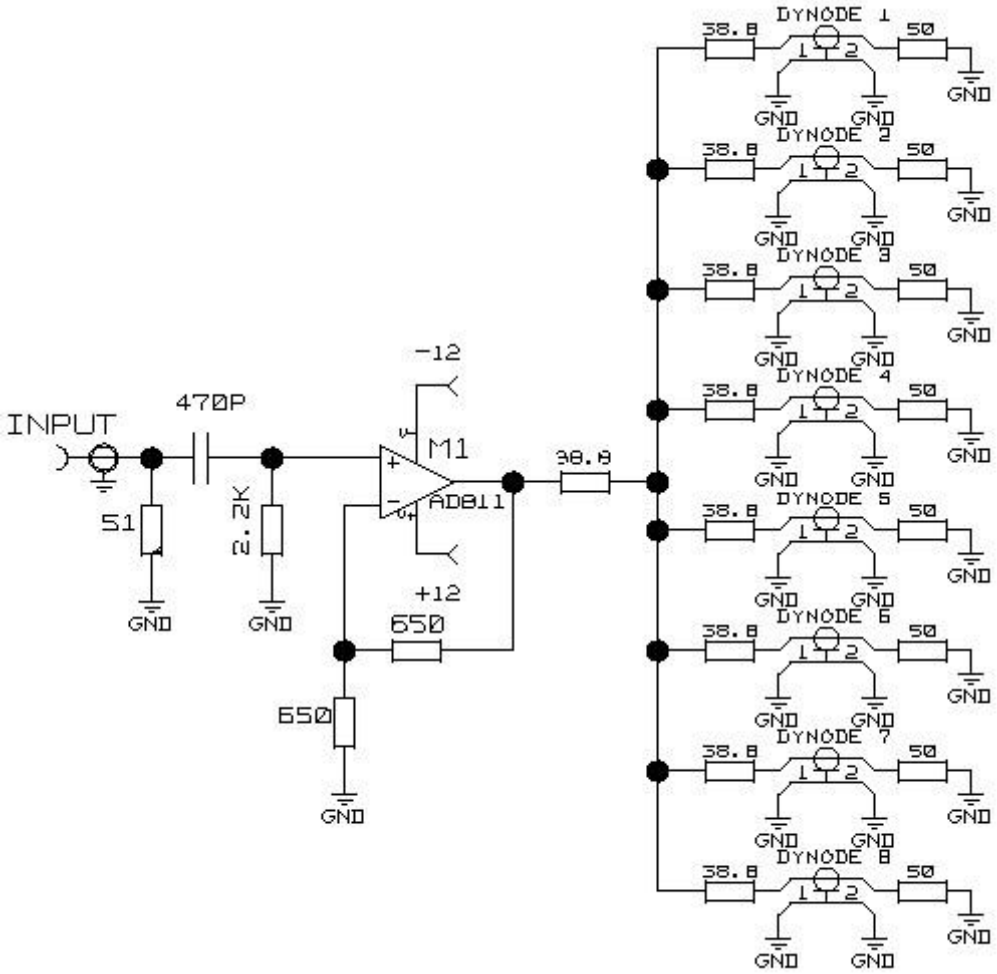

Figure 18: Schematic of the analog signal injection circuit.

reduction of its bandwidth. The output signal has then a slower rise time (high frequency cut-off) and present a drop of its maximum. The solution to keep a fast rising time as well as the input amplitude is to insert a capacitance in parallel for each input of the Op Amp. Moreover a capacitance of high value, 1 μF, is implemented at each stage in order to avoid an increase of the signal offset due to the presence of active components. The capacitance together with the 1 kΩ load of the Op Amp results in a low frequency cut-off at 160 Hz which is quite lower than the frequency we need to transmit. In this way no deformation of the signal is obtained.

The measurements of the total delay times are shown in figure 19 and are summarised in table 8. We have checked that even when lowering the input signals, which would correspond to a particle with an energy lower than 100 GeV, the total delay stays below 100 ns. With an additional delay of 15 ns induced by the D flip-flop and the LVDS driver we obtain a fast trigger answer in less than 120 ns.

Threshold ≈ 40 mV

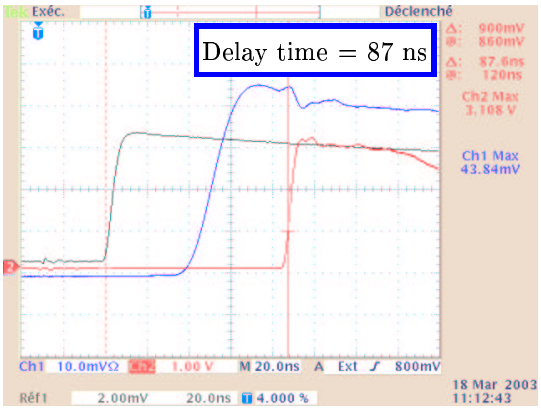

Threshold ≈ 80 mV

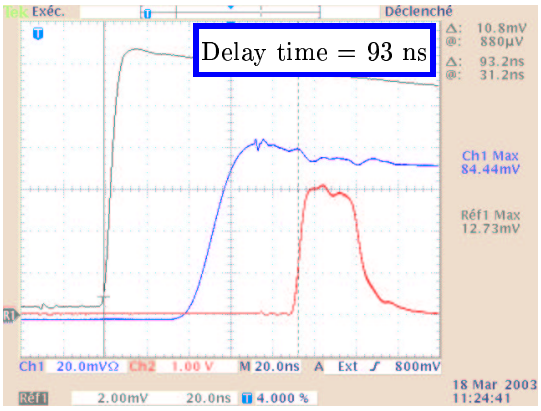

Threshold ≈ 160 mV

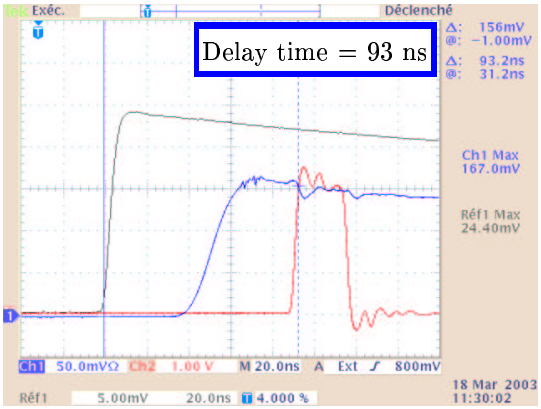

Threshold ≈ 400 mV

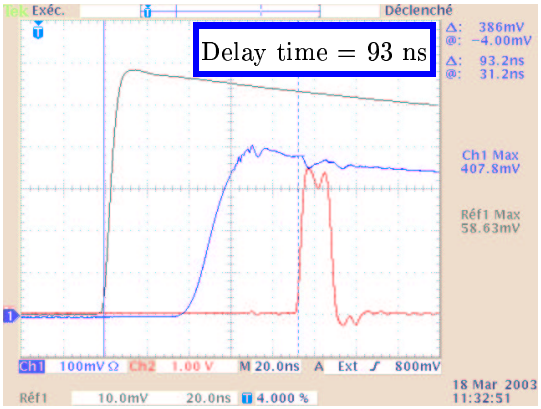

Threshold ≈ 1 V

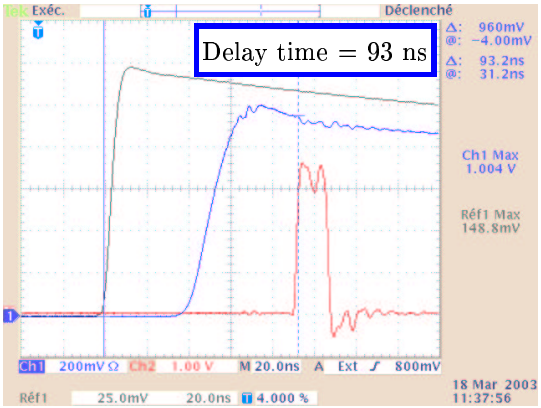

Threshold ≈ 1.8 V

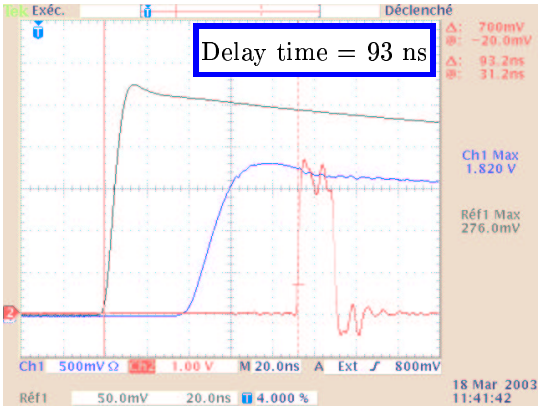

Figure 19: Timing results of the analog sum for the 6 thresholds. The dynode signal is in black, the input of the comparator in blue and its output in red.

Energy Threshold	Comparator Threshold	Delay
2 GeV	40 mV	87 ns
4 GeV	80 mV	93 ns
8 GeV	160 mV	93 ns
18 GeV	400 mV	93 ns
48 GeV	1V	93 ns
90 GeV	1.8V	93 ns

Table 8: Delay at the end of the analog sum for the 6 energy thresholds.

Input amplitude ≈ 20 mV

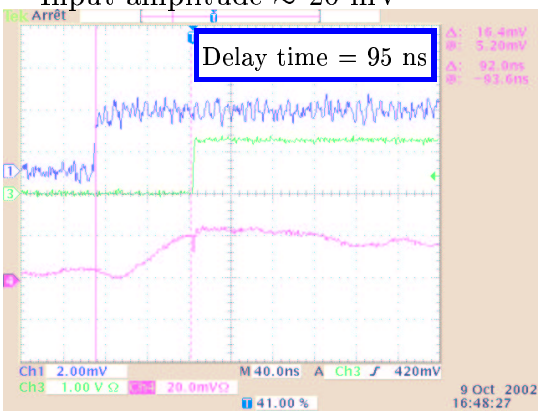

Input amplitude ≈ 150 mV

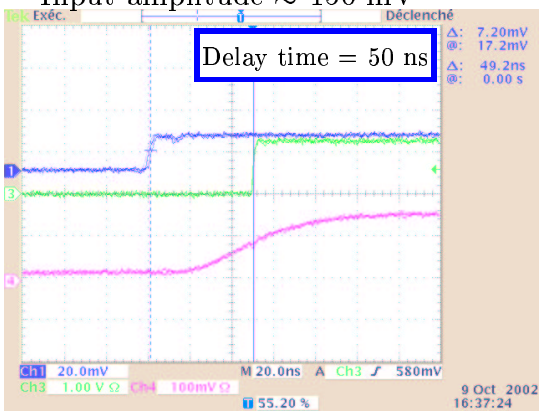

Input amplitude ≈ 3 V

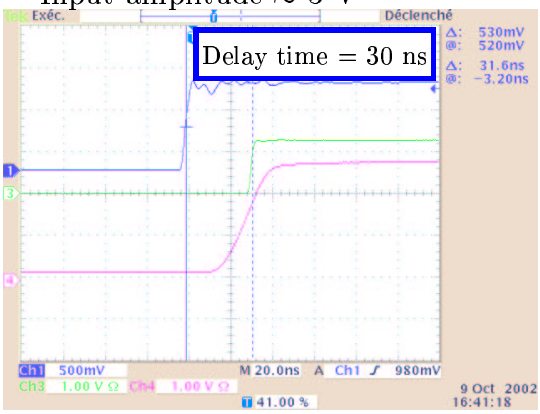

Figure 20: Timing results of WIDTH circuit for the column threshold at 15 mV in the case of a 20mV, 150mV, and 3V analog input signal. The dynode signal is in blue, the input of the comparator in pink and its output in green.

WIDTH Delay

The column threshold for the WIDTH circuit will be chosen between 90 MeV and 100 MeV. This corresponds to a 18 to 20 mV signal for the 4 dynodes with a gain of 10. To estimate the delay of the WIDTH circuit we have set the comparator threshold to 15 mV and feed signals of 20 mV, 150mV and 3 V. The corresponding delays amount 95 ns, 50 ns and 30 ns respectively. If the column comparator is validated by an energy threshold of 2 GeV (delay around 120 ns) all column hits will be active before the validation. With additional 15 ns delay induced from the D flip-flop this lets about 900 ns for the digital signal processing.

4 Conclusion

The presented algorithm for a stand-alone gamma trigger allowed to lower the threshold energy to 2 GeV. The efficiency reaches 97 % for 3 GeV photons and is above 99 % for photons of 5 GeV or more. The corresponding trigger rate from cosmic protons amounts to less than 40 Hz. The robustness of the trigger algorithm was tested and has shown that in most of the cases the efficiency is stable for photons above 3 GeV. Thanks to the flexibility of the algorithm a loss of efficiency can be recovered by adjusting the threshold. The changes in the rate stay always in the standard specification with a maximum rate of 110 Hz in the worst case.

The technical studies have demonstrated the feasibilities of the gamma trigger project. The answer of the fast trigger based on the analog sum is obtained in less than 120 ns. The determination of the column hits is performed in parallel so that about 900 ns are left for the digital signal processing. Including redundancy the power consumption is below 12 W for the complete ECAL trigger system.

Acknowledgment

We would like to thank the GAM team of Montpellier with whom this project was built. We would also like to thank the INFN-Sezione di Pisa group who produced most of the data samples used in this study. With both teams we had very fruitful discussions which helped the advancement of our studies. Finally we would like to thank Emmanuel Bouhana who, during his internship at LAPP, played a great part in the technical final design.

References

[1] **Studies for a stand-alone photon trigger using the Electromagnetic Calorimeter.** C. Goy and S. Rosier.

AMS Note 2001-06-04.

[2] **A proposal for a low energy gamma trigger (algorithm and rates)** M. Sapinski, A. Favard and A. Jacholkowska. AMS Note 1002-11-03

[3] **MC Simulation of AMS-02 Level-1 Trigger.** Evgueny Choumilov AMS Note 2001-06-05.

[4] **Protons in Near Earth Orbit.** The AMS Collaboration Phys. Letter B472 (215-226).

[5] **Cosmic Protons.** The AMS Collaboration Phys. Letter B490 (27-35).

[6] **Participation à la conception et à la réalisation du système électronique de déclenchement du calorimètre électromagnétique de l'expérience AMS.** E. Bouhana, R.Hermel Juin 2002.